Mass-Flux Characteristics of Tropical Cumulus Clouds from Wind Profiler Observations at Darwin, Australia

VICKAL V. KUMAR

School of Earth, Atmosphere and Environment, Monash University, Melbourne, Victoria, Australia

CHRISTIAN JAKOB

School of Earth, Atmosphere and Environment, and Australian Research Council Centre of Excellence for Climate System Science, Monash University, Melbourne, Victoria, Australia

ALAIN PROTAT

Centre for Australian Weather and Climate Research, Melbourne, Victoria, Australia

CHRISTOPHER R. WILLIAMS

University of Colorado Boulder, and NOAA/Earth System Research Laboratory/Physical Sciences Division, Boulder, Colorado

PETER T. MAY

Centre for Australian Weather and Climate Research, Melbourne, Victoria, Australia

(Manuscript received 8 September 2014, in final form 30 December 2014)

ABSTRACT

Cumulus parameterizations in weather and climate models frequently apply mass-flux schemes in their description of tropical convection. Mass flux constitutes the product of the fractional area covered by convection in a model grid box and the vertical velocity in cumulus clouds. However, vertical velocities are difficult to observe on GCM scales, making the evaluation of mass-flux schemes difficult. Here, the authors combine high-temporal-resolution observations of in-cloud vertical velocities derived from a pair of wind profilers over two wet seasons at Darwin with physical properties of precipitating clouds [cloud-top heights (CTH), convective–stratiform classification] derived from the Darwin C-band polarimetric radar to provide estimates of cumulus mass flux and its constituents. The length of this dataset allows for investigations of the contributions from different cumulus cloud types—namely, congestus, deep, and overshooting convection—to the overall mass flux and of the influence of large-scale conditions on mass flux. The authors found that mass flux was dominated by updrafts and, in particular, the updraft area fraction, with updraft vertical velocity playing a secondary role. The updraft vertical velocities peaked above 10 km where both the updraft area fractions and air densities were small, resulting in a marginal effect on mass-flux values. Downdraft area fractions are much smaller and velocities are much weaker than those in updrafts. The area fraction responded strongly to changes in midlevel large-scale vertical motion and convective inhibition (CIN). In contrast, changes in the lower-tropospheric relative humidity and convective available potential energy (CAPE) strongly modulate in-cloud vertical velocities but have moderate impacts on area fractions. Although average mass flux is found to increase with increasing CTH, it is the environmental conditions that seem to dictate the magnitude of mass flux produced by convection through a combination of effects on area fraction and velocity.

1. Introduction

Cumulus clouds play an important role in weather and climate by maintaining the large-scale atmospheric circulation (e.g., Fritsch 1975; Emanuel et al. 1994), transporting heat, moisture, and momentum in the

Corresponding author address: Vickal V. Kumar, Centre for Australian Weather and Climate Research, Australian Bureau of Meteorology and CSIRO, GPO Box 1289, Melbourne VIC 3001, Australia.
E-mail: v.kumar@bom.gov.au

DOI: 10.1175/JAS-D-14-0259.1

atmosphere (Yanai et al. 1973) and producing a multitude of clouds (e.g., Liu and Zipser 2005). Recent studies indicate the existence of distinct types of cumulus clouds in the tropics (e.g., Johnson et al. 1999; Kumar et al. 2013a). These are shallow cumulus with cloud-top heights (CTH) near the trade inversion layer 1–3 km above the surface, cumulus congestus clouds with CTH in the midlevels between 3 and 7 km, deep cumulonimbus clouds with CTH between 7 km and the base of the tropopause layer (~15 km for the topics), and overshooting convection with tops extending into the tropopause layer.

Individual cumulus clouds, particularly deep and overshooting modes, are generally thought to contain convective-scale (1–10 km) updraft and downdraft cores. Observations reveal that cumulus updraft and downdraft flow characteristics differ in several ways (e.g., Knupp and Cotton 1985; Sun et al. 1993). Updrafts are triggered by convergence of environmental airflow and typically start near the cloud base. They dominate in the growing and mature phases of cumulus clouds (Paluch and Knight 1984). Entrainment processes and water loading reduce updraft strength, while latent heating (e.g., Zipser 2003) and precipitation (e.g., Fierro et al. 2009; Heymsfield et al. 2010) enhance updraft strength. In contrast, downdrafts commonly occur in the mature and decaying phases of cumulus clouds. Mature-phase downdrafts generally occur above the freezing level and they are forced by convergence of air detrained from the tops of the updrafts with slower-moving ambient air (Smull and Houze 1987; Sun et al. 1993), whereas decay-phase downdrafts typically occur below the freezing level and are forced by precipitation loading, evaporation, and melting (May and Rajopadhyaya 1999).

In general circulation models (GCMs) convection cannot be represented by modeling individual convective clouds. Instead, simple representations of the collective effects of a cumulus cloud ensemble existing in a model grid box are applied. Among the most widespread of these cumulus parameterization approaches is the so-called mass-flux approach [see Arakawa (2004) for an overview]. Here, the vertical transport by the cloud ensemble is directly related to the mass flux through the clouds, itself a product of the air density, the fractional area covered, and the vertical velocity in cumulus updrafts and downdrafts. While conceptually simple, the evaluation of mass-flux approaches from observations has proven difficult, as measurements of the area fraction and vertical velocities in updrafts and downdrafts on the scale of a GCM grid box are difficult to ascertain. As a result, much of the evaluation of mass-flux schemes has relied on the use of cloud-resolving models (e.g., Randall et al. 2003; Derbyshire et al. 2004; Petch et al. 2014).

The main motivation of this study is to close this obvious observational gap and to demonstrate the potential of using existing observational dataset for evaluating model mass-flux schemes. In particular, we wish to address the following two questions: 1) What is the observed vertical structure of convective mass flux and which of its constituents (area or velocity) dominate the overall structure? 2) How sensitive is mass flux to changes in the environmental conditions?

There are previous observational studies that determined direct in-cloud mass fluxes. Numerous in situ aircraft penetrations conventionally provide the best insights in convective cloud dynamics (e.g., Byers and Braham 1949; Marwitz 1973; LeMone and Zipser 1980; Anderson et al. 2005). However, to facilitate evaluation of mass-flux schemes in a GCM, longer temporal length of continuous convective profiling are needed, such as those from advanced remote sensing techniques. Examples of long-term in-cloud mass-flux observations include the works of May and Rajopadhyaya (1999) and Giangrande et al. (2013), where they used wind profiler retrievals from a tropical and subtropical site, respectively. Both studies found the peaks in updraft speeds and updraft core widths associated with deep convection occurred in upper levels, near 10-km altitude. In contrast, downdrafts peaked near the cloud base. In the tropics, updraft cores have smaller speeds but are wider compared to the subtropics. Heymsfield et al. (2010), who investigated deep convection in both the tropics and subtropics using airborne Doppler radars, also reported similar characteristics in vertical velocities for updrafts and downdrafts.

To extract mass flux over a GCM-size grid, we need direct measurements of vertical velocities inside every cumulus cloud enclosed by the model grid box. Most commonly, this is achieved using a dual-Doppler radar retrieval technique (e.g., Collis et al. 2013). However, the dual-Doppler approach requires at least two radars, with the accuracy of retrieved vertical velocity depending on the location in the radar domain. An alternative and more direct approach to determine vertical velocity is to use a wind profiler (May and Rajopadhyaya 1999; Williams 2012). The current study will be using the latter approach using data collected in Darwin, Australia, for the two wet seasons (November–April) of 2005/06 and 2006/07. The main difficulty in using wind profiler observations is that they represent a single atmospheric column and temporal aggregation is required to represent larger spatial areas. By comparing the wind profiler cloud occurrences with volumetric radar data, we demonstrate that the statistical aggregation of single-column profiler measurements over a longer period do depict

convection comparable to that which will be observed in a GCM-size grid box. We then proceed to determine both the fractional area and in-cloud velocities in convective updrafts and downdrafts using the profiler information and aggregate them into GCM-equivalent mass-flux profiles.

Having determined profile of mass flux from observations over a GCM-size box, we evaluate the sensitivity of the vertical structure and strength of the mass flux to environmental conditions [lower-tropospheric (0–5 km) moisture, CAPE, and CIN] and large-scale vertical motions. The Darwin wet season experiences a wide variety of convective systems owing to the presence of two distinct convective regimes: active monsoon–oceanic conditions and buildup–break continental conditions (e.g., Pope et al. 2009; Kumar et al. 2013b). This makes Darwin a good location to investigate the sensitivity of mass flux to varying environmental conditions. Kumar et al. (2013b) showed that the main influence on convection in the Darwin area was the large-scale meteorological conditions. However, they also found that the underlying surface type also plays a role and as a result the effect of the surface type (coastal in this case) on the observed cumulus mass-flux characteristics cannot be ignored and will require a cautious approach when using these results for GCM evaluations.

Past studies have attempted similar sensitivity tests of mass-flux profiles (or the constituents of mass flux) to the synoptic regimes and environmental conditions using both observations and simulations. Cifelli and Rutledge (1994, 1998), using wind profiler–observed vertical velocity statistics, found significant differences in the mean vertical motion between Darwin break and monsoon storms, with evidence of a bimodal peak in the vertical velocity profile for break cases, while the monsoon cases had a more uniform profile. Here we will extend these studies to more detail by contrasting the mass flux and its constituents as a function of different large-scale environmental conditions. In particular, we will investigate the sensitivity of observed mass flux to the low-level (0–5 km) tropospheric humidity and qualitatively compare the results to those of the idealized cloud-resolving model (CRM) simulations in Derbyshire et al. (2004). These simulations implied that in a dry environment, the mass flux decreases monotonically with height above the cloud base, leading to the formation of mostly shallow convection. Moist environments, on the other hand, led to deep convection with the peak mass flux located at an elevated height in the midtroposphere.

The paper is structured as follows. Section 2 introduces the datasets used in the study. Section 3 describes the method to retrieve velocity and area profiles from wind profiler observations and establishes these single-column observations when averaged in time provide a good proxy for mass flux in a GCM-size grid box. Section 4 presents the main results of the study, including the mean mass-flux profile and its variability, its sensitivity to environmental conditions, and the contributions from different cumulus types to the overall mass flux. This is followed by a summary and discussion in section 5.

2. Data

The main goal of this study is to provide observational estimates of convective mass flux and its constituents at a scale relevant to the parameterization of convection in GCMs as well as its sensitivity to environmental conditions. This requires the use of a variety of datasets. Specifically, we make use of a pair of wind profilers embedded in the field of view of scanning C-band dual-polarization radar (CPOL; Keenan et al. 1998) and combine those with detailed estimates of the large-scale conditions provided by a variational analysis algorithm. Each of these data sources are explained in turn below.

a. The Darwin wind profiler radar pair

We use data collected by a 50- and 920-MHz wind profiler pair from two Darwin wet seasons (October 2005–April 2006 and October 2006–April 2007), recorded at 1-min resolution. The main advantage of using this data source is that wind profilers provide more accurate estimates of in-cloud vertical velocity than other remote sensing techniques, including dual-Doppler radar techniques (e.g., Collis et al. 2013). The disadvantage is that measurements are taken at a single point, but frequently in time, and a time–space conversion is required to make them useful to study the mass-flux behavior on scales of a GCM grid box.

Here, vertical velocities are computed by applying the dual-frequency algorithm developed in Williams (2012) to the Doppler returns from the vertical beams of the 50- and 920-MHz wind profiler pair. The beamwidth of the vertical beam is approximately 0.2 km at 1-km height and increases to 2 km by 10-km height. The wind profiler pair was synchronized to begin their vertical beam observations every 1 min. The full description of the Darwin wind profiler setting can be found in Williams (2012).

The 50-MHz profiler simultaneously observes both Bragg scatter from ambient air, which provides a direct measurement of the vertical velocity of air parcels (wanted signal) and Rayleigh scatter from hydrometeors (unwanted signal). If signals from the two

scattering processing are not properly separated, then the vertical-air-motion estimates will be biased downward because of contamination from falling hydrometeors. The Williams (2012) method uses the spectra from the 920-MHz profiler, which are sensitive to mainly hydrometeor returns, to remove the Rayleigh echo returns from the 50-MHz profiler spectra. The filtered 50-MHz signal is then processed using the standard wind profiling processing technique described in Carter et al. (1995) and is based on the profiler online processing (POP) routine. The POP routine estimates the spectrum noise level, the spectrum signal start and end integration points, and the first three moments: power, mean reflectivity-weighted Doppler velocity, and the spectrum width (equal to twice the spectrum standard deviation). The mean Doppler velocity corresponds to the vertical air motion. The accuracy of the vertical velocity retrieval by the Darwin wind profiler pair is estimated to be between 0.05 and 0.25 $m\,s^{-1}$ using a Monte Carlo simulation design (Williams 2012). Further comparisons between the Darwin wind profiler and statistical techniques for the separation of terminal fall velocity and vertical air velocity also yielded an agreement to within 0.1–0.15 $m\,s^{-1}$ (Protat and Williams 2011).

The profiler vertical velocity measurements are interpolated onto a vertical grid of 100-m resolution over an altitude range of 1.7–17 km. However, the highest-quality data is thought to be limited to heights below 11 km (May and Rajopadhyaya 1999) because of the reduction in profiler sensitivity with height. Moreover, the spreading of the profiler beam leads to increase in velocity uncertainties with changing height. These uncertainties can be lowered by temporal averaging of the data.

Finally, the vertical velocity data from the wind profiler was further filtered to keep only measurements that were in cumulus clouds (see section 3 for more detail). To achieve this, we need to know (i) if cumulus clouds occurred over the profiler and ii) the CTH of these cumulus clouds. These two cloud properties are extracted from the CPOL radar, which contains the wind profilers within its field of view, roughly 24 km southwest from the radar location [see Fig. 1 of May et al. (2002)]. The CPOL measurements are introduced in more detail in the following subsection. Vertical velocities outside cumulus clouds are not considered here.

b. Darwin CPOL radar

We use measurements of reflectivity from the CPOL radar, which have been sampled onto a cubic grid with a horizontal grid size of 2.5 km × 2.5 km and vertical resolution of 0.5 km. The horizontal scanning area of CPOL is approximately 70 000 km^2, sufficient enough to contain few GCM-size grid boxes.

Specifically, this study makes use of two physical characteristics of precipitating clouds derived from the CPOL reflectivities:

(i) We apply a convective versus stratiform classification and use only those precipitating clouds identified as convective over the wind profiler to extract their mass-flux characteristics. The Steiner algorithm (Steiner et al. 1995) is used to identify convective clouds at the CPOL pixel collocated with the wind profiler location. This algorithm has been successfully employed in previous studies (e.g., Kumar et al. 2013a,b; Penide et al. 2013). As the CPOL radar takes 10 min to complete a full volume scan, all 1-min scans of the wind profiler falling into a 10-min interval of convective cloud occurrence over the profiler are used as valid measurements of vertical velocity.

(ii) As our focus is on convective mass flux, we filter out any vertical velocity measurements taken in cirrus anvils and/or in clear air above active convective drafts. To do so we make use of the 0-dBZ echo-top height (0-dBZ ETH) extracted from the CPOL reflectivity profile over the profiler site. Previous studies have shown that the 0-dBZ echo tops from C-band radar observations are usually within 1 km of cloud-top heights estimated by millimeter cloud radars such as that on *CloudSat* (Casey et al. 2012) or on the ground at Darwin (Kumar et al. 2013a). To ensure that we study continuous updrafts or downdrafts, we require that there is vertically continuous reflectivity signal between the lowest CPOL level of 2.5-km height and the 0-dBZ echo top. We also apply the echo-top height to classify the observed precipitating cumulus cell as congestus, deep, or overshooting (Kumar et al. 2013a, 2014), allowing us to investigate the contribution to the total mass flux from the various cumulus modes.

In summary, we use CPOL data for four purposes: 1) to identify convective cloud incidences at the profiler site, 2) to remove vertical velocity measurements taken in clear air above the convective towers, 3) to separate the convective clouds into three cumulus modes, and 4) to validate area fractions derived from vertically pointing measurements against that obtained with volumetric data (more details in section 3).

c. Background environmental conditions

Apart from providing overall mass-flux estimates, we also aim to examine the effects of the environmental conditions on the mass-flux behavior. To do so requires

reliable observational estimates of key environmental parameters. Here we use 6-hourly information on lower-tropospheric (0–5) km relative humidity ($RH_{0–5}$), convective available potential energy (CAPE), convective inhibition (CIN), and the large-scale vertical motion at 500 hPa (ω_{500}). We use two main sources to derive these parameters.

$RH_{0–5}$ is extracted from the Darwin airport operational radiosoundings. We simply average the relative humidity measurements between 0 and 5 km. The remaining three parameters—CAPE, CIN, and ω_{500}—are from a large-scale dataset derived for the Darwin region by Davies et al. (2013) by applying the variational budget analysis technique of Zhang and Lin (1997) using numerical weather prediction (NWP) analysis data as ''pseudoradiosondes'' and radar and satellite observations at the surface and top of the atmosphere, as suggested by Xie et al. (2004). By comparing their approach to results from the Tropical Warm Pool International Cloud Experiment field study (May et al. 2008), Davies et al. (2013) showed that this technique provides much better estimates of the large-scale state of the atmosphere than the direct use of analyses or reanalyses from NWP centers.

The median over the two wet seasons for $RH_{0–5}$, CAPE, CIN, and ω_{500}, respectively, were 74%, 548 J kg^{-1}, 43 J kg^{-1}, and -0.38 hPa h^{-1}. Note that a negative value for vertical motion represents upward motion. Likewise, the 90% interval (i.e., between the 5% and 95% levels about the medians) for $RH_{0–5}$ measurements were between 43% and 96%, for CAPE were between 0 and 1410 J kg^{-1}, for CIN they were 9 and 243 J kg^{-1}, and for ω_{500} they were between -6.67 and 3.81 hPa h^{-1}. These values set the range for which our results can likely be compared with GCMs.

3. Method

The main motivation of this study is to provide a statistical picture of mass-flux profiles using observations, which will then be useful to evaluate existing cumulus mass-flux schemes in models and assess the respective contributions of convective area fraction and vertical velocity to mass flux. Ideally, this would require high-resolution observations of vertical velocity both in time and space over a volume of 100 km × 100 km in the horizontal and 20 km in the vertical (typical GCM grid box). No such measurements exist. As outlined in the introduction, this study makes use of vertical velocity retrievals from dual-frequency wind profiler observations. However, we will combine the wind profiler information with that from the scanning CPOL radar to investigate the representativeness of the single-site measurements for convection over a GCM-size grid.

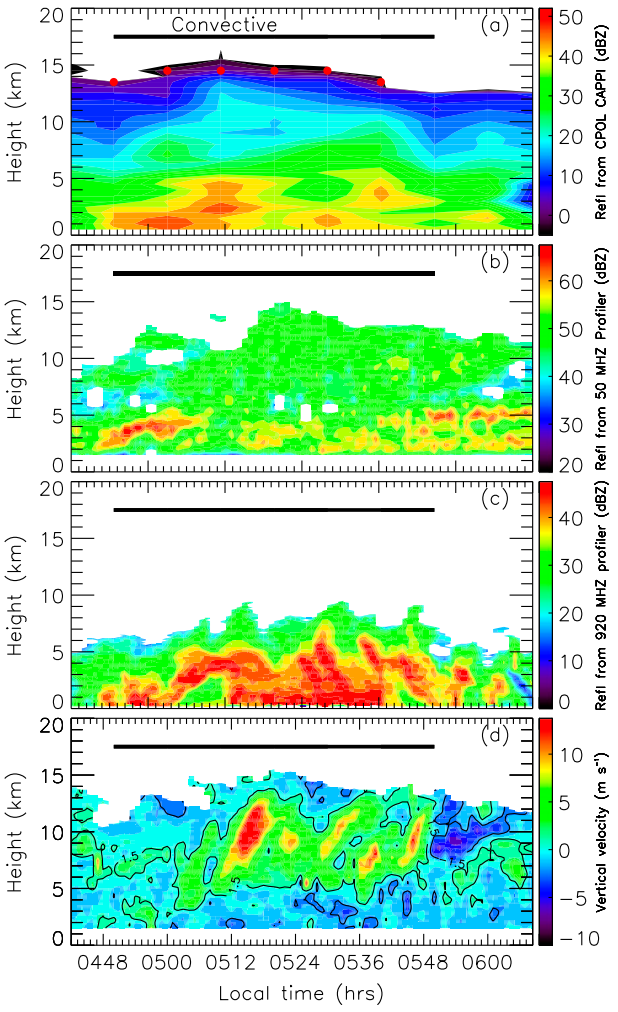

FIG. 1. Overshooting convection captured by the wind profiler around 0500 LT 21 Mar 2006. (a) Time–height section of CPOL reflectivity collocated with the profiler in bins of 10 min in time and 0.5 km in height. The red dots are the 0-dBZ ETH of Steiner-classified convective columns. (b)–(d) Reflectivity from the 50- and 920-MHz profilers, and retrieved profiler vertical velocities, respectively. The profiler data are displayed in finer bins of 1 min in time and 0.1 km in height.

While our overall goal is to provide a statistical study of several hundred cumulus cells occurring over time in a GCM box, we first illustrate our methodology to derive vertical motion and area fraction profiles using a snapshot of a deep convective case observed concurrently by both radar types shown in Fig. 1. Figure 1a shows the time–height cross section of reflectivity from the CPOL radar at the profiler site, which is available in 10-min time intervals and 0.5-km resolution in height. The remaining panels of Fig. 1 show the wind profiler measurements. The profiler observations are available at a much finer resolution of 1 min in time and 0.1 km in height. The red circles in Fig. 1a depict the 0-dBZ ETH

locations at those times where the Steiner classification finds a convective cloud over the profiler site (also indicated by the black line).

The differences between the CPOL reflectivities (Fig. 1a) and the 50- (Fig. 1b) and 920-MHz (Fig. 1c) wind profiler reflectivities are found to be quite large, with the CPOL reflectivities in better agreement with the 920-MHz wind profiler reflectivities than with the 50-MHz wind profiler reflectivities. This is not surprising, as the 50-MHz wind profiler reflectivities are a mixture of echoes from clear air and hydrometeors, while CPOL is only sensitive to hydrometeors. The differences between CPOL and the 920-MHz reflectivities likely reflect the high temporal evolution of the convective event within the sampling resolution of CPOL (10 min), which is captured by the 920-MHz observations at 1-min resolution.

Examinations of CPOL radar loops for the event described in Fig. 1 revealed that the overshooting convective system sampled in Fig. 1 was embedded in widespread stratiform clouds and the whole system was moving across the profiler from the southwest. The time–height sections of vertical velocity (Fig. 1d) indicate that the storm was present over the profiler location for approximately 1 h. The regions with vertical motion exceeding $1.5\,\mathrm{m\,s^{-1}}$ (strong updrafts) and $-1.5\,\mathrm{m\,s^{-1}}$ (strong downdrafts) are shown by the black contours. The upward motions first occur at the low levels (3 km) around 0500 LT, which appear to gradually shift to mid- and upper levels. Between 0520 and 0550 LT, the updrafts remain constantly strong between 5 and 15 km. After 0550 LT, there is a secondary increase in upward motions at around 7 km. By this time, the main convective cell had passed over the profiler and the profiler is now sampling the stratiform anvils of the storm as indicated by the absence of convective clouds in Steiner classification applied to CPOL (Fig. 1a).

While present in Fig. 1, it is evident that downdrafts occur much less frequently and with much weaker magnitudes than updrafts. This is well known and has been illustrated in other studies using radar profiler measurements (e.g., May et al. 2002; Heymsfield et al. 2010; Giangrande et al. 2013). The observed regions of downdrafts, although short lived (so smaller spatial width), are consistent with the different downdraft types known to exist (e.g., Knupp and Cotton 1985; Sun et al. 1993). Downdrafts forming at low levels, which are more frequent than downdrafts in upper levels, are likely to be associated with precipitation loading, evaporation, and melting and can be seen throughout the active storm phase. Several downdrafts can be found above the freezing level, such as the observed strongest downdraft around 0540 LT between 7 and 10 km and short-lived downdraft preceding the main updraft shaft at 0500 LT. These upper-level downdrafts can occur both ahead and behind the convective updrafts and their physical cause are suggested to be quite distinct from those downdrafts that occur in lower levels (Sun et al. 1993). These are thought to be air forced, initiated by convergence between air detrained from the tops of the updrafts and slower-moving ambient air (Smull and Houze 1987). There is tendency that these upper-level downdrafts are positively buoyant, whereas the lower-level downdrafts are negatively buoyant (Sun et al. 1993). It is clear from the case study illustrated in Fig. 1 that vertical motions vary significantly over the storm lifetime with cloud height and also between convective and stratiform structures. We do not attempt to study the evolution of vertical velocities as a function of storm lifetime because the profiler may be sampling only a section of individual storms.

To be of use for model evaluation, the derived mass-flux profiles must be representative for an area the size of a GCM grid box. To account for all cumulus clouds over the model size grid requires computation of convective area fraction. The area fraction is typically defined as the ratio of the size of all convective cells in the domain over the total domain size. Scanning radars, such as CPOL, are most suitable to calculate area fraction using this spatial sampling approach. Since we wish to compute mass flux from a vertically pointing wind profiler, which takes measurements over a column with a small cross-sectional area, the area fraction cannot be directly estimated using these measurements. Instead, convective area fraction is determined as the ratio of the time CPOL identifies convection above the profiler over the total sampling time. We use a long total sampling time of two wet season with the rationale that the convection, at a point, derived from this long time series is a good sample of that occurring in the entire domain over the same sampling time.

To evaluate this approach, the area fractions were derived as described above using both the scanning CPOL and vertically pointing wind profiler, respectively (Fig. 2). Recall that only convective cloud columns from CPOL are used to calculate both the spatial statistics from CPOL and the temporal statistics at the profiler site. The convective area fraction from CPOL was calculated for various circular regions of radius ranging from 10 to 100 km centered on the wind profiler site. The CPOL area fractions for three selected domain sizes shown in Fig. 2 are remarkably similar. This suggests that convection experienced at the profiler site is a good approximation for convection experienced in a GCM-size grid box centered on the wind profiler location. Importantly, the convective area fraction derived from

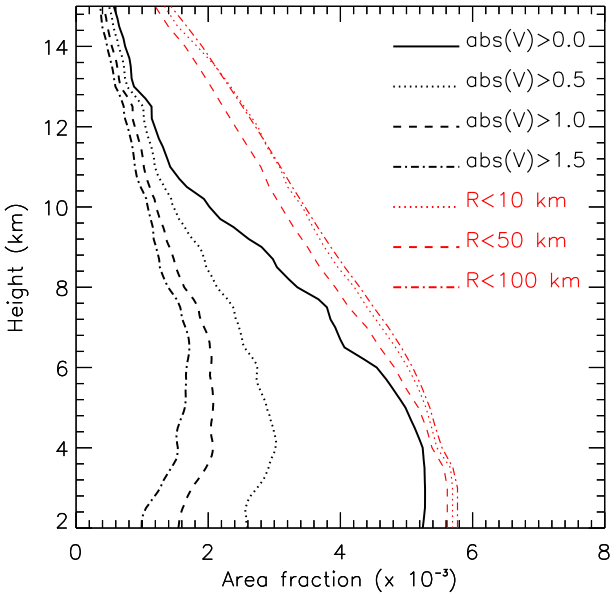

FIG. 2. The two-wet-season-mean profile of convective area fractions using vertically pointing observations from the profiler (black) and volumetric observations from CPOL (red). As explained in the text, profiler area fractions were extracted by applying the "time approach" on different absolute vertical velocity thresholds ranging from 0 to 1.5 m s^{-1}. The area fractions from CPOL are extracted using the "space approach" for different circular regions of radii ranging from 10 to 100 km, centered over the profiler.

the wind profiler for the whole time period (solid curve, $|v| \geq 0\,\mathrm{m\,s^{-1}}$) shows a similar structure as the area fraction from CPOL in the lower and middle troposphere but drops off more rapidly above 8 km. The CPOL radar takes 10 min to complete each volumetric scan, so when present it is assumed that the convection will last for the entire 10 min. The example discussed in Fig. 1 shows that the temporal variability is high within 10 min, with large differences observed between CPOL and 920-MHz reflectivities. In contrast, the wind profiler samples every 1 min, so even though a 10-min window is classified as convective by CPOL, the individual ten 1-min profiles from the wind profiler do not always contain valid vertical velocity measurements. Inevitable instrumental problems may have further contributed to this. Also, at higher altitude, the profiler area fraction begins to drop relatively rapidly compared to the CPOL fractions owing to the drop in profiler sensitivity with altitude. The CPOL sensitivity does not change much with height.

We further evaluate the area fraction estimates from the profiler by applying consecutively larger thresholds to the vertical velocity measurements. The thresholds of $|v| > 0.5$, 1.0, and 1.5 m s^{-1} are chosen as they have been employed by previous investigators to identify updraft and downdraft cores with profiler observations (e.g., LeMone and Zipser 1980; May et al. 2002; Giangrande et al. 2013). Increasing the velocity selection threshold leads to larger difference in area fractions from the two radars, particularly below the freezing level. Thus, to achieve convective area fractions with the profiler approach that is closest to the area fractions obtained with the CPOL radar, all vertical velocity data points (i.e., $|v| > 0\,\mathrm{m\,s^{-1}}$) from the identified convective intervals will be used herein. This will likely result in values of mean vertical velocity that are much lower than those reported in previous studies, which generally used velocity thresholds to remove the low velocity values from their analysis.

Equipped with estimates of area fraction and in-cloud vertical velocity from the profiler measurements, we can now calculate the mass flux M_c (kg s^{-1} m^{-2}). Here, M_c is defined using the traditional GCM-type definition for mass flux by considering all cumulus cloud occurring over a large area:

$$M_c = \rho\sigma_u v_u + \rho\sigma_d v_d, \tag{1}$$

where ρ is the air density (kg m^{-3}) and σ_u is the area fraction of updraft cores in the grid box and is a dimensionless quantity (σ_u can be further subdivided into the number of cores and the width of cores), v_u is the mean velocity of updraft (m s^{-1}), and σ_d and v_d are the area fraction and mean velocity of the downdraft cores, respectively.

The vertical profile of air density is computed using standard textbook formulas, with input temperature and pressure fields extracted from the Darwin radiosoundings. The mean profiles of all remaining variables in Eq. (1) are computed using the profiler vertical velocity data from the convective intervals. We found that unlike the area fraction, the mean mass-flux profile was largely independent of the different velocity threshold (not shown). This is because larger vertical velocity thresholds lead to smaller area fractions (Fig. 2) but much larger mean vertical velocities, with the two effects compensating and leading to similar mean mass-flux values.

4. Results

a. *Overall characteristics of convective mass flux and its constituents*

1) MEAN MASS-FLUX PROFILE

Precipitating convective clouds were identified by the CPOL radar over the profiler site for a total of 283 ten-minute scans during the two wet seasons analyzed here. This corresponds to a convective area fraction near the

TABLE 1. The two-wet-season occurrence frequency of congestus, deep, and overshooting clouds, and separately for the four environmental conditions.

Environmental conditions	Total of the 1-min wind profiler scans			
	Congestus (CTH < 7 km)	Deep (7 ≤ CTH ≤ 15 km)	Overshooting (CTH > 15 km)	All cumulus clouds
$RH_{0-5} \leq 68\%$	145	196	148	489
$68\% < RH_{0-5} < 82\%$	228	557	184	969
$RH_{0-5} \geq 82\%$	292	741	337	1370
CAPE ≤ 365 J kg^{-1}	251	620	184	1055
365 < CAPE < 747 J kg^{-1}	305	540	222	1067
CAPE ≥ 747 J kg^{-1}	109	334	263	706
CIN ≤ 30 J kg^{-1}	527	1030	512	2069
30 < CIN < –62 J kg^{-1}	78	346	127	551
CIN ≥ 62 J kg^{-1}	60	118	30	208
$\omega_{500} \leq -1.82$ hPa h^{-1}	485	1232	649	2366
$-1.82 < \omega_{500} < 1.24$ hPa h^{-1}	109	176	10	295
$\omega_{500} \geq 1.24$ hPa h^{-1}	71	86	10	167
All	665	1494	669	2828

surface of approximately 0.5%. Note that this represents an average including many instances with no convection present in the domain for significant periods of time. It is therefore not comparable to convective area fractions found in previous studies (e.g., Davies et al. 2013), which reach values up to 10% but reflect instantaneous conditions rather than long temporal averages. Going back to the overall time average, Table 1 summaries the contributions to the total convective area fraction from congestus (CTH < 7 km), deep (CTH between 7 and 15 km), and overshooting clouds (CTH > 15). It also shows the variability of convective cloud frequency in different environment and large-scale terciles. The results shown in Table 1 are discussed further in sections 4a(2) and 4a(3).

Mean profile of the overall mass flux as well as upward and downward mass-flux profiles are shown in Fig. 3. Here, the lower x axis represents the overall mean over the entire two seasons including the very frequent times (99.5%) of no convective clouds present over the profiler site. To provide at least a rough estimate of the values of mass flux "when present," a value more useful to modelers, we average mass fluxes over 3-h windows and discard all windows with no presence of convective clouds (~93%). These results are indicated by the upper x axis in Fig. 3. A 3-h window translates to a grid size of roughly 60 km; calculations are based on 5 m s^{-1} average propagating speed of convective cells (Kumar et al. 2013b). Note that removing zeros will not affect the profile shape but only its magnitude. The overall mean mass flux (thick curve) increases steadily from near cloud base to peak at 6 km just above the freezing level and thereafter decreases gradually with height. At all height levels, except at very high altitudes, mass-flux totals are dominated by updrafts (thin curve). Importantly, these observational results also validate those reported in many studies using cloud-resolving models (e.g., Derbyshire et al. 2004; Kuang and Bretherton 2006) and are also in good agreement with previous attempts to retrieve mass fluxes from profiler observations (e.g., May and Rajopadhyaya 1999).

2) MEAN AREA FRACTION AND VERTICAL VELOCITY

Equation (1) indicates that updraft and downdraft mass fluxes are affected by three fundamental factors: the number of cores, the size of the cores, and the vertical velocity in the cores. The product of the number and size terms divided by domain size gives the area fraction. We now examine the characteristics of these three fundamental factors with the aim to understand the relative contributions of these factors to the mass-flux totals.

We begin by examining the variations in convective area fraction (thick solid line in Fig. 4a) divided into upward area fraction (thin solid line) and downward area fraction (dashed line). Once again we show the overall period averages with the lower x axis and those for 3-h windows that contain convection with the upper x axis. At low levels, updraft and downdraft area fractions are nearly equal. The updraft fraction remains more or less constant from near the surface to 8 km and then decreases steadily at higher levels. Starting from the top, the small downdraft fraction increases slightly to just above the freezing level, where a significant increase in downdraft fraction occurs, indicating the potential importance of this level in downdraft formation. In Figs. 4c and 4d, the upward and downward area fractions (shaded) are subdivided into the number of cores (solid lines) and

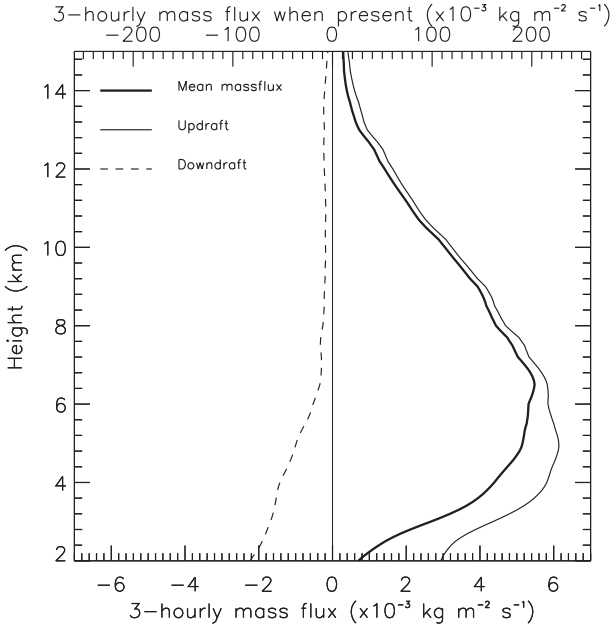

FIG. 3. The two-wet-season-mean vertical profile of overall mass flux (thick curve), updraft mass flux (thin curve), and downdraft mass flux (dashed curve). As explained in the text, mass-flux values were computed using the traditional GCM definition. The upper x axis represents mass-flux values provided there was at least one cumulus cloud in the 3-hourly window (~60 km in spatial width).

their size (dashed line). The core width is measured in minutes and represents the number of consecutive 1-min periods with vertical motion greater than $0\,m\,s^{-1}$ for an updraft core. Downdraft cores are defined analogously using downward motion.

The mean core spatial width associated with upward motion (dashed line in Fig. 4c) increases gradually from an average of ~2 min at cloud base to a maximum average width of ~6 min at a height of 8 km. Assuming a propagation speed of $5\,m\,s^{-1}$, this translates into a width of ~600 m near cloud base and ~1.8 km at midlevels. Above 8 km, the updraft core width decreases sharply. In contrast, the core frequency associated with updrafts is highest near cloud base, decreasing monotonically with increasing height. The net effect of this pattern in updraft width and frequency is that the upward area fraction (shaded region in Fig. 4c) is highest and constant between cloud base and 8 km. Downdraft number increases downward with a particularly sharp increase near the freezing level. The average width of downdraft cores is ~3 min and remains fairly constant with height. Once again assuming a $5\,m\,s^{-1}$ propagation speed, this translates into a size of ~900 m.

The mean vertical velocity (thick black curve in Fig. 4b) increases gradually with height and peaks near $4\,m\,s^{-1}$ at 12 km. This mean profile is the sum of the velocities in updrafts (thin black curve in Fig. 4b) and downdrafts (dashed black curve) weighted by the fractional area of updraft and downdraft cores. The updraft velocity evolution with height is very similar to the overall mean with a drop between 2 and 3 km followed by a steady increase to values of $\sim 5\,m\,s^{-1}$ at high levels. In contrast, the downdrafts show much weaker velocities of $\sim 1\,m\,s^{-1}$, which are almost constant throughout the cloud layer with slightly large values near the tops of very deep clouds.

The mean vertical velocity values shown in Fig. 4b are much lower than those reported elsewhere (e.g., May and Rajopadhyaya 1999; Heymsfield et al. 2010; Giangrande et al. 2013). This is because we do not apply any threshold for the inclusion of the observed in-cloud velocities in our sample of convective drafts, whose existence is instead determined by the CPOL radar measurements over the profiler site [see section 2a(2)]. To enable a more meaningful comparison with previous studies, Fig. 4b shows not only the averages, but also the full 2D histogram of vertical velocity distributions. The 90th percentile of updraft and downdraft velocities (white curves in Fig. 4b) reached up to 15 and $-6\,m\,s^{-1}$, respectively. The profile of the 90th percentile velocities are consistent, both in magnitude and in vertical structure, with the values for land-based deep convection reported in Heymsfield et al. (2010), who only examined the profiles of the maximum updraft and downdraft velocity. May and Rajopadhyaya (1999) and Giangrande et al. (2013) removed velocities between −1.5 and $1.5\,m\,s^{-1}$ from their analysis, but the strongest velocity profiles in those studies compare well with our results. In situ aircraft penetrations results reported in LeMone and Zipser (1980) showed 90th percentile values of around $5\,m\,s^{-1}$ in middle levels. These lower values are likely due to the more continental character of the convection sampled here as well as a possible undersampling of strong convection by aircrafts due to safety concerns.

Next, we reconcile the vertical structure of the mass flux (Fig. 3) with area fraction (Figs. 4a,c,d) and vertical velocity (Fig. 4b). As it is difficult to mentally sum all contributing factors to the total mass flux, we compare the updraft and downdraft terms separately. The increase in updraft mass flux between 2 and 5 km is largely a reflection of the vertical velocity increase combined with a small increase in area fraction. The large reduction in updraft mass flux above 8 km is due to the strong decrease in area fraction, which is slightly offset by an increase in vertical velocity. Note that the decrease in density with height also affects the mass-flux profile, such that constant velocity and area fraction would still imply a reduction of mass flux with height. As the downdraft velocities are small and relatively constant with height, the strong increase in downdraft mass

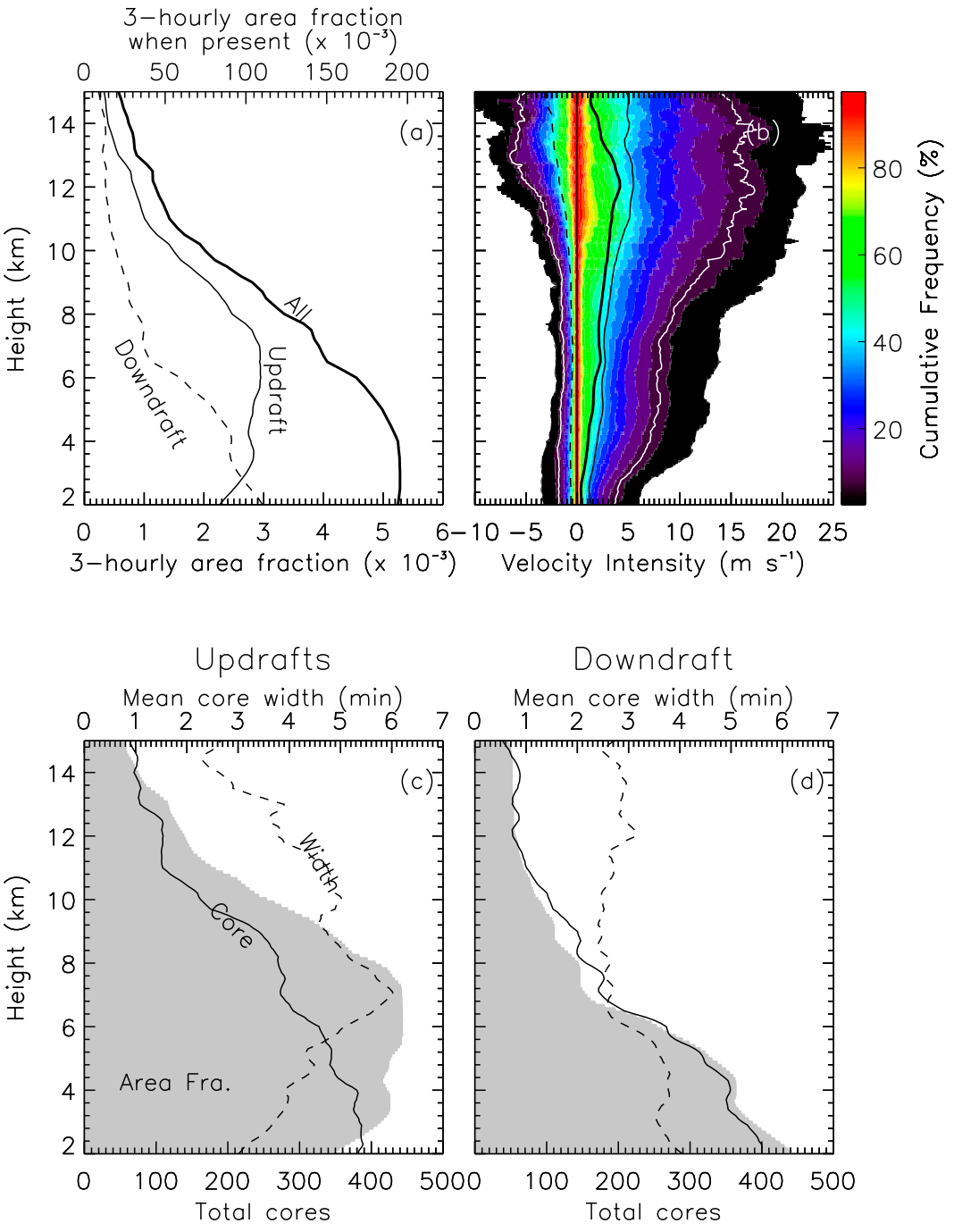

FIG. 4. As in Fig. 3, but for profiles of (a) mean area fraction, (b) mean vertical velocity, (c) cumulative count of updraft cores and mean spatial width, and (d) the downdraft core and width characteristics. The colored plot in (b) is the full 2D cumulative histogram of vertical velocity distributions using bins of 0.5 km in height and 0.2 m s^{-1} in velocity. The white curves are the 90th percentiles in updrafts and downdrafts.

flux below 6 km (Fig. 3) is to first order driven by the corresponding increase in downdraft area fraction.

Overall, perhaps with the exception of increase in updraft mass flux at low levels, the total mass flux is governed to first order by the area fraction. If confirmed at other locations, this would provide the opportunity of estimating the first-order characteristics of mass flux from area fraction alone—a quantity that is much more easily measured using instruments both on the ground and in space than vertical motions.

b. *Sensitivity of mass flux to environmental and large-scale conditions*

Of key relevance to cumulus parameterization is the connection of mass flux with the environmental conditions in which the convection is embedded. In this section, we examine the relationships of $RH_{0–5}$, CAPE, CIN, and ω_{500} with the updraft mass flux, upward area fraction, and upward velocity. As the downdraft contribution to overall mass flux is relatively small, we focus on updraft behavior only.

For the analysis shown in this section, the environmental conditions are grouped into terciles of their respective probability density functions. This ensures that the wind profiler sampling time in each tercile is identical. Note, though, that the amount of convective clouds observed in each tercile can still vary significantly depending on how favorable the conditions in each tercile are for convection. The tercile boundaries for each environmental variable, the amount of time with which convective clouds occur in each tercile, and their subdivision into congestus, deep, and overshooting modes are shown in Table 1.

1) EFFECT OF 0–5-KM RELATIVE HUMIDITY

A moist environment, which is represented by the upper tercile of $RH_{0–5}$, is thought to be important to support the formation of deep convection over its shallower counterparts (e.g., Redelsperger et al. 2002; Derbyshire et al. 2004; Takemi et al. 2004). The results shown in Figs. 5a–c reveal several interesting differences between dry (solid curves, $RH_{0–5} < 68\%$) and moist (dashed curve, $RH_{0–5} > 82\%$) condition updraft mass flux (Fig. 5a), area fraction (Fig. 5b), and velocity (Fig. 5c). The updraft mass flux (Fig. 5a) in dry conditions exhibits a sharp peak at the height of 6 km with a strong dropoff in mass flux above that level, while in moist conditions a smoother and deeper mass-flux profile is evident. The behavior in dry conditions likely indicates the prevalence of shallower clouds [see section 4b(3)]. The updraft area fraction is much smaller in dry conditions, indicative of a less frequent occurrence of convection (see also Table 1). As seen before for the overall means (Figs. 3 and 4), area fraction increases from cloud base to midlevels, followed by a decrease higher up. Vertical velocity increases with height in both states of $RH_{0–5}$. Perhaps surprisingly, the velocities are stronger in dry conditions than in moist conditions, partly compensating the lower mass-flux strength induced by the lower area fractions in that state. The higher velocities can be understood by the need to produce stronger updrafts to penetrate through the dry atmosphere, while in moist conditions weaker updrafts occur more frequently and can penetrate higher into the moist troposphere more easily.

2) EFFECT OF CAPE

Next we study the relationship of mass flux to CAPE (Figs. 5d–f). The differences in the upper- ($>747\,J\,kg^{-1}$; dashed) and lower-tercile ($<365\,J\,kg^{-1}$; solid) CAPE conditions are much smaller than those for $RH_{0–5}$. The mass flux is slightly weaker in low-CAPE conditions and it reaches higher levels in high-CAPE conditions. Somewhat paradoxically, low-CAPE conditions give rise to higher area factions. This is consistent with the findings of Kumar et al. (2013b), who showed that low-CAPE conditions are associated with more frequent but shallower convective clouds over Darwin. The air parcels in the convective clouds are less buoyant in low-CAPE conditions, leading to weaker updraft speed (Fig. 5f) and often shallower cloud. In contrast, in high-CAPE condition, convection is much deeper because the air parcels have greater growth momentum. While less frequent in high-CAPE conditions, convection that occurs exhibits significantly larger vertical velocities. The net effect is that the updraft mass flux at all heights, except near cloud base, is higher in high-CAPE conditions compared to low CAPE conditions.

3) EFFECT OF CIN

In general, when the CIN of the atmosphere is low, more convective cloud systems are likely to form. This is confirmed by our analysis of mass flux in the lowest ($<30\,J\,kg^{-1}$; solid) and highest ($>62\,J\,kg^{-1}$; dashed) CIN terciles (Figs. 5g–i). There is a large difference in mass flux between high- and low-CIN conditions, which is entirely caused by differences in area fraction, which is synonymous with the frequency of occurrence of convection. The vertical velocity profiles are largely unaffected by the state of CIN, indicating that CIN is more likely a predictor for the existence of convection than its strength.

4) EFFECT OF LARGE-SCALE UPWARD MOTION AT 500 HPA

Similar to CIN, large-scale vertical motion is strongly related to the existence of convection (Figs. 5j–l). Almost all convective events occur in the ''lower'' tercile, which comprises large-scale upward motion ($\omega_{500} \leq -1.82\,hPa\,h^{-1}$; solid), while the upper tercile of large-scale downward motion ($\omega_{500} \geq 1.24\,hPa\,h^{-1}$; dashed) is more or less void of convection. The very small fraction (7%) of convective systems that do form when there is large-scale downward motion tend to have very high upward vertical velocities in the upper level, although the poor sampling in this class prevents us from drawing any firm conclusions.

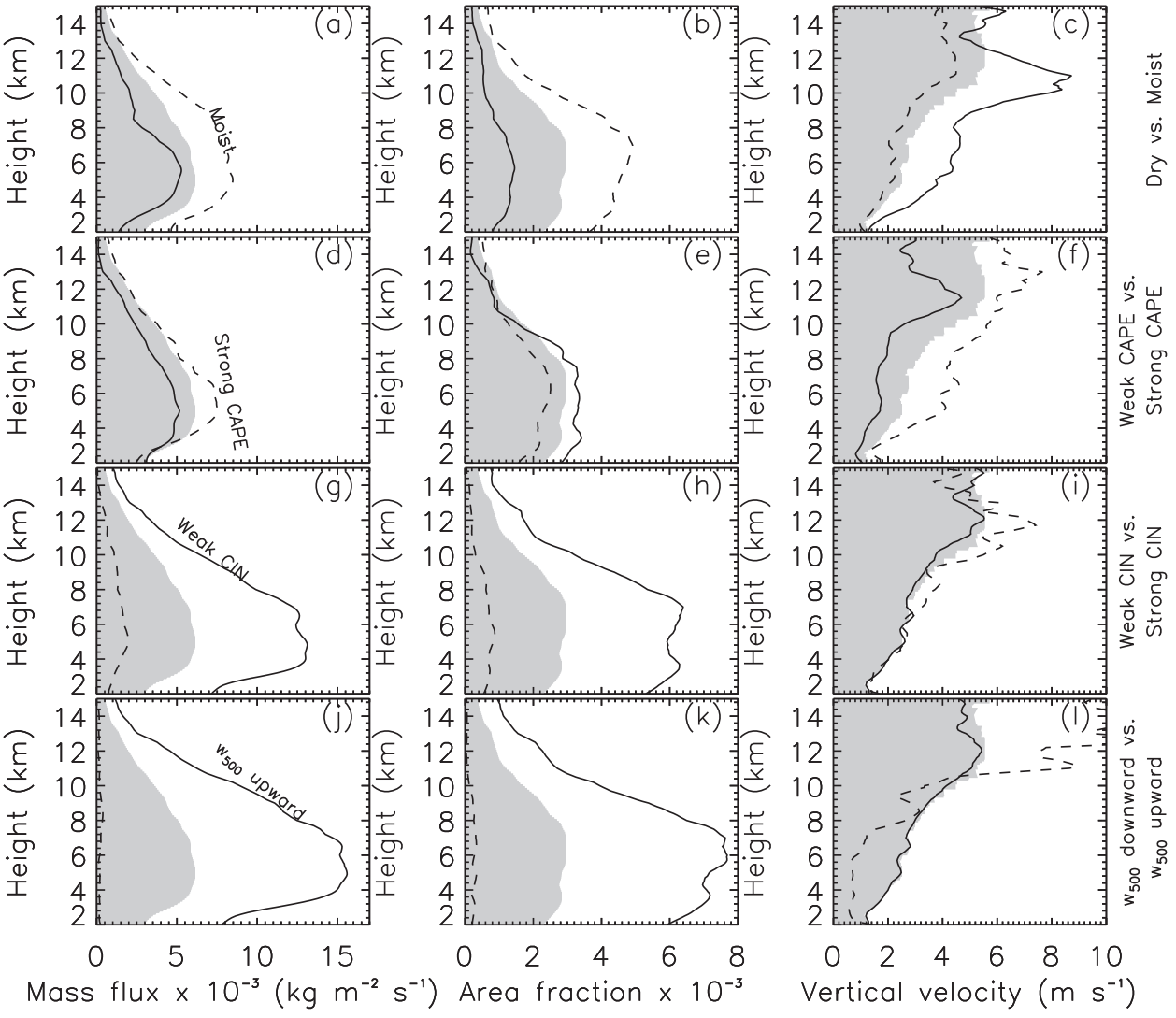

FIG. 5. Effect of (a)–(c) $RH_{0–5}$, (d)–(f) CAPE, (g)–(i) CIN, and (j)–(l) ω_{500} on (left) updraft mass flux, (middle) upward area fraction, and (right) upward vertical velocity intensities. The shaded region is the overall updraft mean without applying any environmental sorting. The solid and dotted lines in each figure correspond to lower and upper terciles of the environmental conditions, respectively. The tercile boundaries are in Table 1.

5) SUMMARY OF EFFECTS OF ENVIRONMENTAL CONDITIONS ON MASS FLUX

In its entirety Fig. 5 provides an important set of lessons about convective behavior that can potentially be used in the construction of cumulus parameterizations. It is clear that different environmental parameters, many of which have been used in constructing elements of existing cumulus schemes, have different effects on the mass flux because they affect its two constituents—area and velocity—in different ways. Large-scale vertical motion and CIN are strongly related to area fraction. These conditions strongly influence the existence and prevalence of convection and through the area fraction exerts a strong control on the convective mass flux. In addition, $RH_{0–5}$ is strongly related to vertical motion in the clouds, although it is likely that there is no direct causality in that relationship. Instead, we speculate that the higher velocities in dry conditions are a result of weaker updrafts not being able to penetrate the dry atmosphere. Changes in CAPE have the least impact on the convective area fraction but instead show a strong relationship with cloud growth dynamics. In low-CAPE conditions, the convective systems tend to be moderately more frequent but with weak updraft speeds while high-CAPE conditions support stronger vertical motions, leading to slightly higher overall mass fluxes in

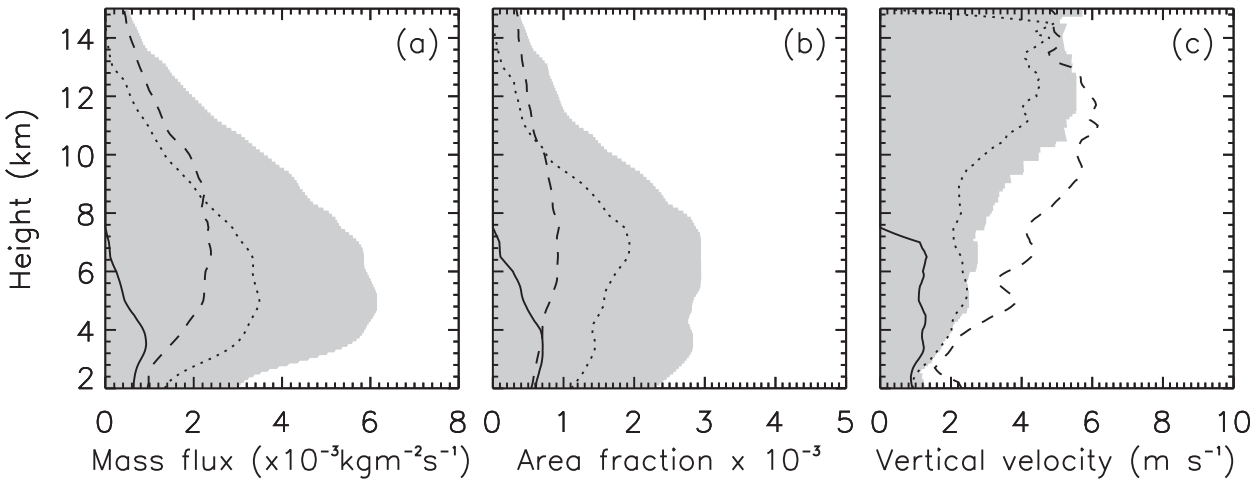

FIG. 6. Contribution to (a) updraft mass flux, (b) upward area fraction, and (c) upward vertical velocity from congestus (solid), deep (dotted), and overshooting (dashed) cumulus clouds. The shaded region represents all cumulus clouds.

high-CAPE conditions. In summary, there is some evidence from Fig. 5 that the constituents of mass flux are responding differently to different environmental conditions, making it difficult to relate mass flux itself to only one of them. This may indicate a potential benefit from treating area and velocity separately in future cumulus parameterization approaches.

c. *Contributions of each cumulus cloud type to the total mass flux in different environmental conditions*

Having investigated the overall mass-flux properties and their relationship to the state of the environment in which the convection is embedded, we now investigate the contributions of individual precipitating cumulus cloud modes—namely, congestus, deep, and overshooting clouds—to the overall cumulus mass flux. The three cloud modes are defined by tracking convective cells and identifying their 0-dBZ ETH (Kumar et al. 2013a, 2014). Cells that never exceed 7 km are classified as congestus, those that exceed 15 km are classified as overshooting, and the rest are classified as deep convection. Kumar et al. (2013a) noted that these three modes have remarkably different rainfall and drop size characteristics and, thus, it will be worthwhile to examine the mass-flux characteristics of these cumulus modes separately as well as quantify their overall effect.

The breakdown of the total time for which the three cumulus convective modes are found at the profiler site is shown in Table 1. We find that the most frequent type of convection sampled by the profiler is deep convection, with just over half of all cases in this category. The other two types contribute roughly one quarter each to the overall sample.

The mean profile of upward mass flux associated with the three cumulus modes and the constituents of these mass-flux profiles are displayed in Fig. 6. Given its high frequency, the highest contribution to the upward mass flux in the lower 8 km of the troposphere is from the deep mode. The mean vertical velocity intensity of this mode shows intermediate strength updraft velocities of 2–4 m s^{-1} with a bimodal structure with peaks at 6 km and above 10 km. The congestus mode contributes about one quarter of the area fraction below 4 km but, because of its relatively weak upward motion on the order of only 1 m s^{-1}, makes a relatively small contribution to the overall mass flux. The overshooting mode contributes around one quarter to the area fraction below 10 km and dominates the area fraction above 10 km. It shows the strongest vertical motion of the three modes with average values increasing from around 4 m s^{-1} at 5 km to 6 m s^{-1} above 10 km.

As the mass fluxes were shown to be sensitive to the environmental conditions, we next investigate how the relative contribution from the three cloud modes may change with the state of the environment. It was evident from Fig. 5 that ω_{500} and CIN mostly determined the existence of convection, while $RH_{0\text{–}5}$ and CAPE had a more direct influence on its structure. We therefore focus on the latter two parameters and contrast the contribution of the three cumulus modes to mass flux in changing $RH_{0\text{–}5}$ and CAPE conditions. These results are shown in Fig. 7.

The total time of each cumulus mode during the different environmental conditions are given in Table 1. The most notable change in total time of individual cumulus modes with respect to different environment conditions occurs for the overshooting mode when

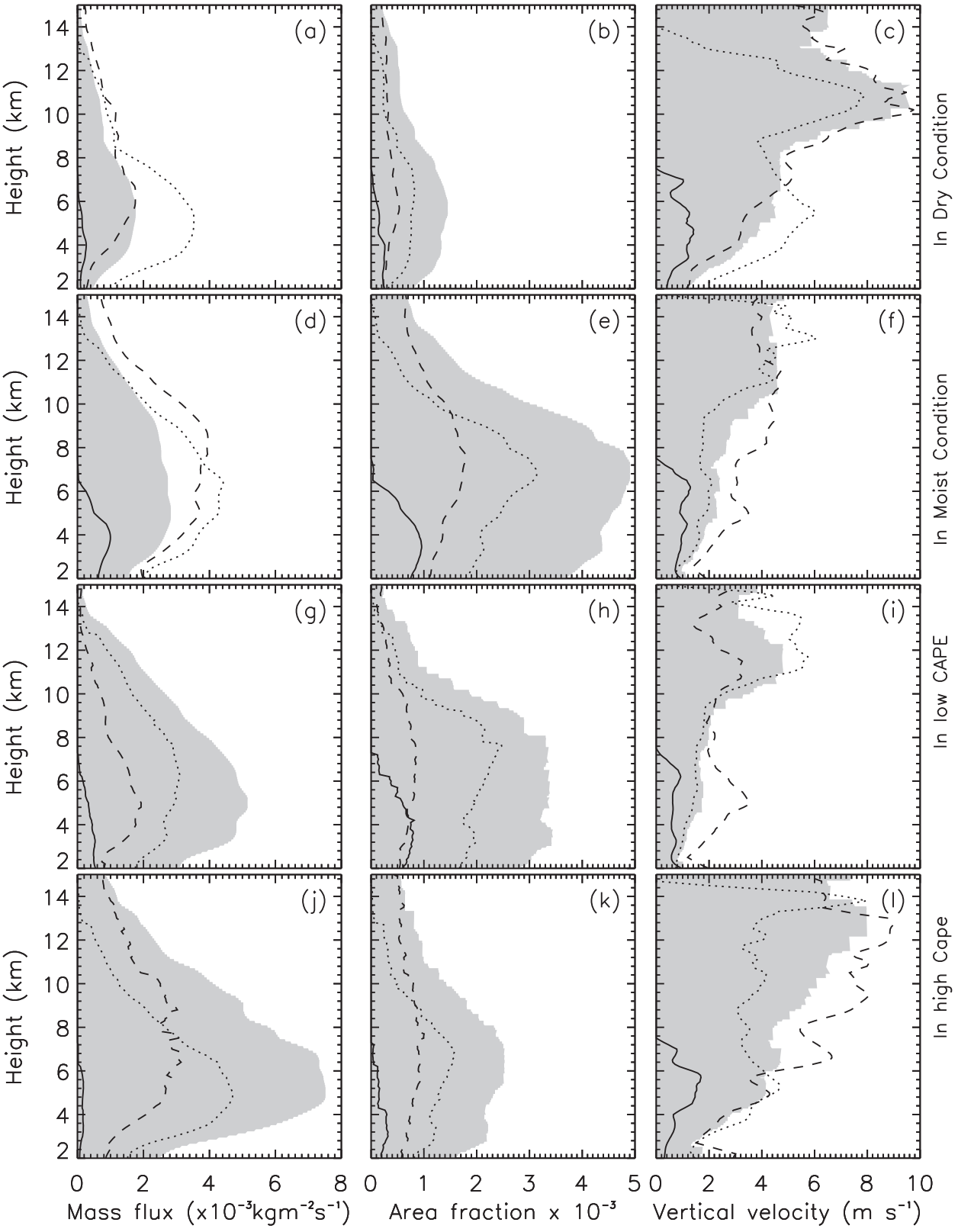

FIG. 7. As in Fig. 6, but for the mean response of the three precipitating cumulus modes in (a)–(c) dry, (d)–(f) moist, (g)–(i) low-CAPE, and (j)–(l) high-CAPE conditions.

sorted with respect to CAPE. While constant in overall terms (Figs. 7h,k), overshooting cloud forms 17% of all convection in low-CAPE conditions but 37% in high-CAPE conditions. This is a result of the occurrence of both the congestus and deep modes decreasing as CAPE increases (Figs. 7h,k). As expected, the vertical velocities for the deep and in particular for the overshooting mode increase with CAPE (Figs. 7i,l), leading to the overall larger mass fluxes in high-CAPE conditions discussed earlier (Fig. 5). We now see that this increase is predominantly driven by an increase in the velocities in the overshooting mode.

Changes in $RH_{0–5}$ (Figs. 7a–f) also strongly affect the overall mix of the occurrence of convective modes. In dry conditions, 60% of the time convection is present is associated with either the congestus or overshooting mode. In contrast, in moist conditions the deep mode becomes the dominant mode occurring 54% of the time. The area of all three convective modes increases significantly in moist conditions (Figs. 7b,e), while the velocities in the deep modes decrease by about half with little change in the congestus mode. This once again highlights that deep convection of both types is stronger but less frequent in dry conditions.

d. Variability in mass-flux measurements

The results shown so far have focused entirely on the mean behavior of mass flux and its constituents, although some indication of variability is revealed by the breakdown into cloud modes and by the 2D histogram of vertical velocity distributions (Fig. 4b). In this section we aim to investigate the variability of mass flux at the typical scale of a GCM grid box across different events, as this is more readily comparable to what the mass-flux parameterization produces. To enable this investigation, we need to compute mass flux over some discrete time window rather than averaging over long periods of time. This once again requires finding a compromise between representing the size of a GCM grid box and the results being affected by the evolution of the convective systems over the time window. We choose a 3-h time-averaging window (~60 km), but we will also contrast our results to those found using a longer 6-h window (~100 km). As most time windows will have no convection at all in them, we focus our investigation on the 95th, 99th, and 99.5th percentiles of the respective distribution functions. Figure 8 shows these percentiles for area fraction (Fig. 8a) and mass flux (Fig. 8b) for both the 3- (green) and 6-hourly (red) time windows. For comparison, we also include the area fractions measured by CPOL in a 50-km radius around the profiler site in Fig. 8a.

While the length of the time window does not affect the mean profile of area fractions, it does affect the variability. Shorter time windows will produce larger variability because there will be increases in incidence of both very large and very small area fractions. Of the 2300 (1150) available 3 (6)-hourly time blocks, 93% (88%) had a convective area fraction of 0. As expected, the upper percentiles of the area fraction distribution yields larger (smaller) values for the 3 (6)-hourly window ranging from 0.05 (0.03) for the 95th percentile to 0.1 (0.08) for the 99th percentile. The 6-hourly window is in closer agreement with the CPOL area fractions.

The upper percentiles of the mass-flux distribution associated with the 3- and 6-hourly windows are shown in Fig. 8b. This figure is in the same format as Fig. 8a, except the the 98th, not the 95th, percentile is shown, as the 95th-percentile mass fluxes were too small to be seen clearly. The 98th-percentile mass flux has the same vertical structure as the mean updraft and downdraft mass-flux profile (Fig. 3), with peak updraft and downdraft mass flux just above the freezing level and close to cloud base, respectively. At higher percentiles, very large updraft mass-flux values occur at higher altitude and are linked with large–vertical velocity events occurring in deep and overshooting convection.

5. Summary and discussion

The aim of this study was to derive convective mass fluxes and their constituents on the scale of a GCM grid box from wind profiler observations and thereby to provide a zeroth-order observational reference for the evaluation of cumulus mass-flux schemes. The analysis conducted characterized the updrafts and downdrafts of precipitating convective clouds with continuous dual-frequency wind profiler observations taken over two wet seasons at Darwin, Australia. We found the net mass flux over the entire measurement period to be positive (upward) between 2- and 14-km heights with a peak near 6 km. The downdraft cumulus mass flux was found to be strongest close to cloud base associated with precipitation loading, with values of less than half of that seen in updrafts.

The separation of mass flux into velocity and area fraction—the latter itself is a product of core width and frequency—showed that the mass flux was most strongly regulated by the area fraction compared to the vertical velocity. While of secondary importance to overall mass-flux magnitude, the vertical velocity intensities revealed some crucial properties related to the cloud dynamics. The convective updraft velocity exhibited a dominant peak in the upper levels (>10 km) and a small secondary peak in the lower level at 6 km particularly associated with the deep convective cloud mode. The observed structures in vertical velocity intensities associated with

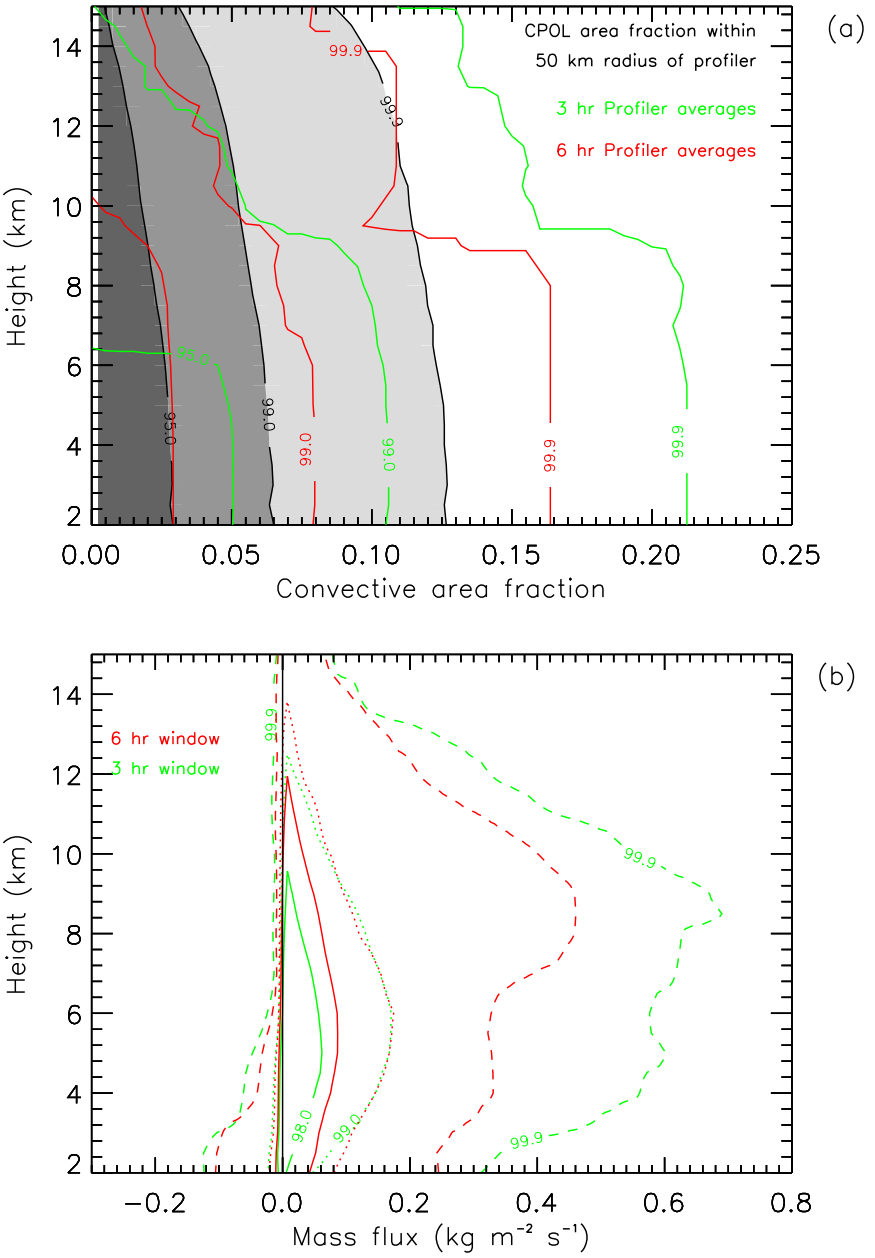

FIG. 8. (a) 2D cumulative histogram of convective area fraction from CPOL over a circular region of radius 50 km centered at the profiler site (gray shaded) and convective area fraction from wind profiler observations over 3- (green) and 6-hourly (red) time windows. (b) As in (a), but for the mass flux.

the deep convection (Figs. 4b and 6) matched well with the updraft profiles reported in previous studies (e.g., May and Rajopadhyaya 1999; Giangrande et al. 2013). The overshooting convective mode had more intense vertical velocity magnitudes than the deep mode at all height levels, increasing monotonically with height.

By separating the mass flux into contributions from different precipitating cumulus types, we demonstrated that a wide variety of vertical velocity intensities and cumulus sizes contributes to the mean mass-flux profile. This was shown to be due to a complex interplay of the frequency, size, and strength of cumulus clouds with the environment. The analysis revealed that approximately 80% of the cumulus population over the two seasons formed when the large-scale vertical motions were strongly upward ($\leq -1.82\,\mathrm{hPa\,h^{-1}}$) and/or when CIN

was small ($\leq 30\,J\,kg^{-1}$). Both low-level relative humidity (RH_{0-5}) and CAPE had a moderate effect on the existence of cumulus clouds but these parameters had a significant impact on the vertical velocity and hence the growth dynamics of clouds. Higher mean velocities were mainly associated with deeper convection that formed in dry ($RH_{0-5} < 68\%$) and high-CAPE conditions (Figs. 5 and 7). While the latter is easily explained by energetic arguments, the former is a less obvious result. We interpret this result as driven by the effects of entrainment of dry air into the clouds limiting the vertical growth of clouds (e.g., Redelsperger et al. 2002). The very few deep cumulus clouds that do succeed to grow in the unfavorable dry conditions need very strong vertical growth momentum and hence display very large vertical velocities.

The downdraft vertical velocities and frequencies were significantly less than those for updrafts at all height levels, except at cloud base and near cloud top, where they were similar. This is consistent with the conceptual picture that a convective cloud is generally made up of one or more dominant updraft cores, which are partly compensated by small and short-lived downdrafts driven by precipitation loading in lower levels and air-forced processes in upper levels (see Fig. 1).

Our study has extended previous investigations of May and Rajopadhyaya (1999) for the tropical Darwin region and Giangrande et al. (2013) for midlatitude central plains of the United States by examining not only the overall mass flux but its constituents at scales relevant to GCM evaluation. Unlike these studies, we accepted all values of vertical motion in our statistical analysis rather than setting a threshold value. This led to better agreement with convective area fraction profile shapes derived from the CPOL scanning radar (Fig. 2), likely making our sample more representative. The mean updraft and downdraft vertical velocity profiles found here are nevertheless in good agreement with earlier studies (e.g., Heymsfield et al. 2010). The sensitivity of mass flux to the environmental moisture conditions is in broad agreement with the modeling study of Derbyshire et al. (2004). Both the observational and model results show that during the moist conditions, the mass flux has a broad peak at midlevels, while in dry conditions, the mass flux decreases monotonically with height; albeit,, this decrease starts at higher levels in the observations (4 km) than in the model simulations (cloud base).

Despite the availability of two wet seasons of observations, perhaps the biggest limitation of our study remains the relatively small sample size. This once again highlights the difficulty of supporting the development of cumulus parameterizations with the relevant measurements. An obvious way to alleviate this problem is to use data from scanning radar systems. Such systems can provide frequent measurements of convective area fractions at GCM-grid-box scale (e.g., Davies et al. 2013) but the challenge is to derive long time series of reliable retrievals of in-cloud vertical velocity from them. This will be the next step of this work. We will use the computationally efficient dual-Doppler retrieval technique from Protat and Zawadzki (1999), which will be evaluated first using the wind profiler vertical velocities as in Collis et al. (2013), but applied to a much longer dataset over Darwin. Our finding that mass-flux profiles tend to be dominated by the convective area fraction and that in-cloud velocities vary with cloud depth may also enable us to derive mass-flux estimates from scanning systems by statistically modeling, rather than measuring, vertical motion and combining those with more easily observed area fractions. This will be the subject of a further study that will extend the first useful foray into supporting cumulus parameterization development more directly with long-term observations presented in this paper.

Acknowledgments. This work has been supported by the U.S. Department of Energy ARM Program (DE-FG02-09ER64742). We would like to acknowledge the contributions of Brad Atkinson and Michael Whimpey in supporting the Darwin observatory and data management. V. Kumar thanks Ed Zipser and two other referees for reviewing this paper.

REFERENCES

Anderson, N. F., C. A. Grainger, and J. L. Stith, 2005: Characteristics of strong updrafts in precipitation systems over the central tropical Pacific Ocean and in the Amazon. *J. Appl. Meteor.,* **44,** 731–738, doi:10.1175/JAM2231.1.

Arakawa, A., 2004: The cumulus parameterization problem: Past, present, and future. *J. Climate,* **17,** 2493–2525, doi:10.1175/1520-0442(2004)017<2493:RATCPP>2.0.CO;2.

Byers, H. R., and R. R. Braham, 1949: The thunderstorm. U.S. Weather Bureau Thunderstorm Project Rep., 287 pp.

Carter, D. A., K. S. Gage, W. L. Ecklund, W. M. Angevine, P. E. Johnston, A. C. Riddle, J. Wilson, and C. R. Williams, 1995: Developments in UHF lower tropospheric wind profiling at NOAA's Aeronomy Laboratory. *Radio Sci.,* **30,** 977–1001, doi:10.1029/95RS00649.

Casey, S. P. F., E. J. Fetzer, and B. H. Kahn, 2012: Revised identification of tropical oceanic cumulus congestus as viewed by CloudSat. *Atmos. Chem. Phys.,* **12,** 1587–1595, doi:10.5194/acp-12-1587-2012.

Cifelli, R., and S. A. Rutledge, 1994: Vertical motion structure in Maritime Continent mesoscale convective systems: Results from a 50-MHz profiler. *J. Atmos. Sci.,* **51,** 2631–2652, doi:10.1175/1520-0469(1994)051<2631:VMSIMC>2.0.CO;2.

——, and ——, 1998: Vertical motion, diabatic heating, and rainfall characteristics in north Australia convective systems.

Quart. J. Roy. Meteor. Soc., **124,** 1133–1162, doi:10.1002/qj.49712454806.

Collis, S., A. Protat, P. T. May, and C. Williams, 2013: Statistics of storm updraft velocities from TWP-ICE including verification with profiling measurements. *J. Appl. Meteor. Climatol.,* **52,** 1909–1922, doi:10.1175/JAMC-D-12-0230.1.

Davies, L., C. Jakob, P. T. May, V. V. Kumar, and S. Xie, 2013: Relationships between the large-scale atmosphere and the small-scale state for Darwin, Australia. *J. Geophys. Res. Atmos.,* **118,** 11 534–11 545, doi:10.1002/jgrd.50645.

Derbyshire, S. H., I. Beau, P. Bechtold, J.-Y. Grandpeix, J.-M. Piriou, J.-L. Redelsperger, and P. M. Soares, 2004: Sensitivity of moist convection to environmental humidity. *Quart. J. Roy. Meteor. Soc.,* **130,** 3055–3080, doi:10.1256/qj.03.130.

Emanuel, K. A., J. D. Neelin, and C. S. Bretherton, 1994: On large-scale circulations in convecting atmospheres. *Quart. J. Roy. Meteor. Soc.,* **120,** 1111–1143, doi:10.1002/qj.49712051902.

Fierro, A. O., J. M. Simpson, M. A. LeMone, J. M. Straka, and B. F. Smull, 2009: On how hot towers fuel the Hadley cell: An observational and modelling study of line-organized convection in the equatorial trough from TOGA COARE. *J. Atmos. Sci.,* **66,** 2730–2746, doi:10.1175/2009JAS3017.1.

Fritsch, J. M., 1975: Cumulus dynamics: Local compensating subsidence and its implications for cumulus parameterization. *Pure Appl. Geophys.,* **113,** 851–867, doi:10.1007/BF01592963.

Giangrande, S. E., S. Collis, J. Straka, A. Protat, C. Williams, and S. Krueger, 2013: A summary of convective-core vertical velocity properties using ARM UHF wind profilers in Oklahoma. *J. Appl. Meteor. Climatol.,* **52,** 2278–2295, doi:10.1175/JAMC-D-12-0185.1.

Heymsfield, G. M., L. Tian, A. J. Heymsfield, L. Li, and S. Guimond, 2010: Characteristics of deep tropical and subtropical convection from nadir-viewing high-altitude airborne Doppler radar. *J. Atmos. Sci.,* **67,** 285–308, doi:10.1175/2009JAS3132.1.

Johnson, R. H., T. M. Rickenbach, S. A. Rutledge, P. E. Ciesielski, and W. H. Schubert, 1999: Trimodal characteristics of tropical convection. *J. Climate,* **12,** 2397–2418, doi:10.1175/1520-0442(1999)012<2397:TCOTC>2.0.CO;2.

Keenan, T. D., K. Glasson, F. Cummings, T. S. Bird, J. Keeler, and J. Lutz, 1998: The BMRC/NCAR C-band polarimetric (CPOL) radar system. *J. Atmos. Oceanic Technol.,* **15,** 871–886, doi:10.1175/1520-0426(1998)015<0871:TBNCBP>2.0.CO;2.

Knupp, K. R., and W. R. Cotton, 1985: Convective cloud downdraft structure: An interpretive survey. *Rev. Geophys.,* **23,** 183–215, doi:10.1029/RG023i002p00183.

Kuang, Z., and C. S. Bretherton, 2006: A mass-flux scheme view of a high-resolution simulation of a transition from shallow to deep cumulus convection. *J. Atmos. Sci.,* **63,** 1895–1909, doi:10.1175/JAS3723.1.

Kumar, V. V., C. Jakob, A. Protat, P. T. May, and L. Davies, 2013a: The four cumulus cloud modes and their progression during rainfall events: A C-band polarimetric radar perspective. *J. Geophys. Res. Atmos.,* **118,** 8375–8389, doi:10.1002/jgrd.50640.

——, A. Protat, P. T. May, C. Jakob, G. Penide, S. Kumar, and L. Davies, 2013b: On the effects of large-scale environment and surface conditions on convective cloud characteristics over Darwin, Australia. *Mon. Wea. Rev.,* **141,** 1358–1374, doi:10.1175/MWR-D-12-00160.1.

——, ——, C. Jakob, and P. T. May, 2014: On atmospheric regulation of the growth of moderate to deep cumulonimbus in a tropical environment. *J. Atmos. Sci.,* **71,** 1105–1120, doi:10.1175/JAS-D-13-0231.1.

LeMone, M. A., and E. J. Zipser, 1980: Cumulonimbus vertical velocity events in GATE. Part I: Diameter, intensity and mass-flux. *J. Atmos. Sci.,* **37,** 2444–2457, doi:10.1175/1520-0469(1980)037<2444:CVVEIG>2.0.CO;2.

Liu, C., and E. J. Zipser, 2005: Global distribution of convection penetrating the tropical tropopause. *J. Geophys. Res.,* **110,** D23104, doi:10.1029/2005JD006063.

Marwitz, J. D., 1973: Trajectories within the weak echo regions of hailstorms. *J. Appl. Meteor.,* **12,** 1174–1182, doi:10.1175/1520-0450(1973)012<1174:TWTWER>2.0.CO;2.

May, P. T., and D. K. Rajopadhyaya, 1999: Vertical velocity characteristics of deep convection over Darwin, Australia. *Mon. Wea. Rev.,* **127,** 1056–1071, doi:10.1175/1520-0493(1999)127<1056:VVCODC>2.0.CO;2.

——, A. R. Jameson, T. D. Keenan, P. E. Johnston, and C. Lucas, 2002: Combined wind profiler/polarimetric radar studies of the vertical motion and microphysical characteristics of tropical sea breeze thunderstorms. *Mon. Wea. Rev.,* **130,** 2228–2239, doi:10.1175/1520-0493(2002)130<2228:CWPPRS>2.0.CO;2.

——, J. H. Mather, G. Vaughan, C. Jakob, G. M. McFarquhar, K. N. Bower, and G. G. Mace, 2008: The Tropical Warm Pool International Cloud Experiment. *Bull. Amer. Meteor. Soc.,* **89,** 629–645, doi:10.1175/BAMS-89-5-629.

Paluch, I. R., and C. A. Knight, 1984: Mixing and evolution of cloud droplet size spectra in a vigorous continental cumulus. *J. Atmos. Sci.,* **41,** 1801–1815, doi:10.1175/1520-0469(1984)041<1801:MATEOC>2.0.CO;2.

Penide, G., V. V. Kumar, A. Protat, and P. T. May, 2013: Statistics of drop size distribution parameters and rain rates for stratiform and convective precipitation during the North Australian wet season. *Mon. Wea. Rev.,* **141,** 3222–3237, doi:10.1175/MWR-D-12-00262.1.

Petch, J., A. Hill, L. Davies, A. Fridlind, C. Jakob, Y. Lin, S. Xie, and P. Zhu, 2014: Evaluation of intercomparisons of four different types of models simulating TWP-ICE. *Quart. J. Roy. Meteor. Soc.,* **140,** 826–837, doi:10.1002/qj.2192.

Pope, M., C. Jakob, and M. Reeder, 2009: Regimes of the north Australian wet season. *J. Climate,* **22,** 6699–6715, doi:10.1175/2009JCLI3057.1.

Protat, A., and I. Zawadzki, 1999: A variational method for real-time retrieval of three-dimensional wind field from multiple-Doppler bistatic radar network data. *J. Atmos. Oceanic Technol.,* **16,** 432–449, doi:10.1175/1520-0426(1999)016<0432:AVMFRT>2.0.CO;2.

——, and C. R. Williams, 2011: The accuracy of radar estimates of ice terminal fall speed from vertically pointing Doppler radar measurements. *J. Appl. Meteor. Climatol.,* **50,** 2120–2138, doi:10.1175/JAMC-D-10-05031.1.

Randall, D. A., and Coauthors, 2003: Confronting models with data - The GEWEX Cloud Systems Study. *Bull. Amer. Meteor. Soc.,* **84,** 455–469, doi:10.1175/BAMS-84-4-455.

Redelsperger, J.-L., D. B. Parsons, and F. Guichard, 2002: Recovery processes and factors limiting cloud-top height following the arrival of a dry intrusion observed during TOGA COARE. *J. Atmos. Sci.,* **59,** 2438–2457, doi:10.1175/1520-0469(2002)059<2438:RPAFLC>2.0.CO;2.

Smull, B. F., and R. A. Houze Jr., 1987: Dual-Doppler radar analysis of a midlatitude squall line with a trailing region of stratiform rain. *J. Atmos. Sci.,* **44,** 2128–2148, doi:10.1175/1520-0469(1987)044<2128:DDRAOA>2.0.CO;2.

Steiner, M., R. A. Houze Jr., and S. E. Yuter, 1995: Climatological characterization of three-dimensional storm

structure from operational radar and rain gauge data. *J. Appl. Meteor.,* **34,** 1978–2007, doi:10.1175/1520-0450(1995)034<1978:CCOTDS>2.0.CO;2.

Sun, J., S. Braun, M. I. Biggerstaff, R. G. Fovell, and R. A. Houze Jr., 1993: Warm upper-level downdrafts associated with a squall line. *Mon. Wea. Rev.,* **121,** 2919–2927, doi:10.1175/1520-0493(1993)121<2919:WULDAW>2.0.CO;2.

Takemi, T., O. Hirayama, and C. Liu, 2004: Factors responsible for the vertical development of tropical oceanic cumulus convection. *Geophys. Res. Lett.,* **31,** L11109, doi:10.1029/2004GL020225.

Williams, C. R., 2012: Vertical air motion retrieved from dual-frequency profiler observations. *J. Atmos. Oceanic Technol.,* **29,** 1471–1480, doi:10.1175/JTECH-D-11-00176.1.

Xie, S., R. T. Cederwall, and M. Zhang, 2004: Developing long-term single-column model/cloud system–resolving model forcing data using numerical weather prediction products constrained by surface and top of the atmosphere observations. *J. Geophys. Res.,* **109,** D01104, doi:10.1029/2003JD004045.

Yanai, M., S. Esbensen, and J. Chu, 1973: Determination of bulk properties of tropical cloud clusters from large-scale heat and moisture budgets. *J. Atmos. Sci.,* **30,** 611–627, doi:10.1175/1520-0469(1973)030<0611:DOBPOT>2.0.CO;2.

Zhang, M., and J. Lin, 1997: Constrained variational analysis of sounding data based on column-integrated budgets of mass, heat, moisture, and momentum: Approach and application to ARM measurements. *J. Atmos. Sci.,* **54,** 1503–1524, doi:10.1175/1520-0469(1997)054<1503:CVAOSD>2.0.CO;2.

Zipser, E. J., 2003: Some view on ''hot towers'' after 50 years of tropical field programs and two years of TRMM data. *Cloud Systems, Hurricanes, and the TRMM, Meteor. Monogr.,* No. 51, Amer. Meteor. Soc., 49–58.